Supplementary Information

Tuning thermomechanical properties of hydrogen-bonded materials by using a mixed cocrystal approach

Gary C. George III,[a] Liulei Ma,[a] Jack R. Gaffney,[a] Richard K. Brooks,[b] Daniel K. Unruh,[c] Ryan H. Groeneman,*[b] and Kristin M. Hutchins*[a,d]

[a] Department of Chemistry, University of Missouri, Columbia, Missouri 65211, United States. Email: kristin.hutchins@missouri.edu

[b] Department of Natural Science and Mathematics, Webster University, St. Louis, Missouri 63119, United States. Email: ryangroeneman19@webster.edu

[c] Office of the Vice President for Research, University of Iowa, Iowa City, Iowa, 52242, United States.

[d] MU Materials Science & Engineering Institute, University of Missouri, Columbia, Missouri, 65211, United States.

1. Materials, General Methods, and Synthesis of the Cocrystals

Materials

4-stilbazole (SB) and the solvent ethanol (reagent grade) were both purchased from Sigma-Aldrich Chemical (St. Louis, MO, USA) and used as received. Additional ethanol (200 proof) was purchased from Decon Labs Inc. (King of Prussia, PA, USA). Sodium bicarbonate, sodium chloride, hexanes, dichloromethane (DCM), chloroform ($CHCl_3$), and ethyl acetate were purchased from Fisher Scientific (Fair Lawn, NJ, USA). Resorcinol and bromine (Br_2) were purchased from Alfa Aesar (Ward Hill, MA, USA). 4,6-Dibromoresorcinol (4,6-diBr res)[1] was synthesized by using a modified literature procedure. 4-(Phenylethynyl)pyridine (PAB)[2] and additional SB[3] were synthesized using literature procedures. All crystallizations were performed in 20 mL scintillation vials.

General Methods

Thin-layer chromatography (TLC) was performed using ALUGRAM Xtra aluminum sheets coated with silica gel from MACHEREY-NAGEL Inc (Germany). Silica gel was purchased from SILICYCLE Inc. (Quebec, Canada). Column chromatography was carried out using silica gel (40-63 μm). Chemical shifts (δ) are reported in ppm relative to residual $CHCl_3$ (^{1}H, δ 7.26). Nuclear magnetic resonance (NMR) spectra for synthesized compounds were collected using Bruker AMX-600 spectrometer at ambient probe temperature, unless otherwise noted. Data for ^{1}H NMR spectra are reported as follows: chemical shift, multiplicity (s = singlet, d = doublet, t = triplet, m = multiplet), coupling constant (*J*, Hz), and integration. Deuterated chloroform for NMR spectroscopy was purchased from Cambridge Isotope Laboratories.

^{1}H NMR spectra for the cocrystals were collected using a Bruker Avance III 500 MHz spectrometer using DMSO-d_6 as a solvent. Powder X-ray diffraction (PXRD) data was collected at room temperature on a Rigaku Miniflex 6G benchtop powder diffractometer using Cu K_α radiation (λ = 1.54059 Å) with an anode voltage of 40 kV, a current of 15 mA, in Bragg-Brentano beam geometry. Diffraction intensities were recorded on a D/teX Ultra position sensitive detector and samples were prepared on zero background holders. The patterns were obtained by scanning a 2θ range between 5˚ to 50˚ with a step size of 0.02°, and a scan time of 5 degrees/min.

TGA was performed on a TA Instruments TGA Q50 operating under a nitrogen atmosphere (40 mL/min) with a platinum pan. Crystal samples were run at a rate of 10 °C/min by heating from room temperature to 400 °C. DSC experiments were conducted using a TA Instruments DSC250 equipped with a RCS 90 refrigerated cooling system and under a nitrogen atmosphere. The flow rate was 50 mL/min, and the heating rate was 10°C/min. The samples were placed in TA zero pans, enclosed using a TA zero Hermetic lid, and crimped using a press. The thermograms were processed using the Trios software. For the DSC experiments, (4,6-diBr res)·2(SB) was heated from room temperature to 160 °C at a rate of 10 °C/min, then isothermally held at 160 °C for 1 min, and cooled back to room temperature at a rate of 10 °C/min. For (4,6-diBr res)·2(PAB) and (4,6-diBr res)·(SB)·(PAB) the samples were heated from room temperature to 150 °C at a rate of 10 °C/min, then isothermally held at 150 °C for 1 min, and cooled back to room temperature at a rate of 10 °C/min. The cutoff temperatures for DSC were chosen to avoid decomposition.

Synthesis of 4,6-diBr res[1]

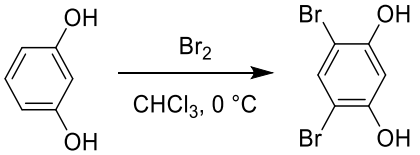

4,6-diBr res

Resorcinol (1.1 g, 10 mmol) and 40 mL of $CHCl_3$ were added into a 250 mL round bottom flask and placed in an ice bath. A solution of Br_2 (3.2 g, 20 mmol) in 20 mL of $CHCl_3$ was added into the flask dropwise. The mixture was stirred at 0 °C for ~1h, then a saturated $NaHCO_3$ solution was added slowly to quench the reaction and remove the excess Br_2. The reaction mixture was washed with brine and water. Then, $CHCl_3$ was removed by distillation under reduced pressure, and the crude product was purified by silica gel column chromatography (hexanes/dichloromethane/ethyl acetate=10:2:1 to 2:2:1, v/v/v). The product **4,6-diBr res** was afforded as a white solid (1.79 g, 66.8% yield). ^1H NMR (600 MHz, $CDCl_3$) δ 7.55 (s, 1H), 6.76 (s, 1H), 5.52 (s, 2H).

Crystallization details

All crystallization experiments were conducted at ambient temperature and humidity. After dissolving the components as detailed below, the vials were left at room temperature, and the solvent was allowed to slowly evaporate.

Crystallization of (4,6-diBr res)·2(SB)

Cocrystals of (4,6-diBr res)·2(SB) were synthesized by dissolving 50.0 mg of SB in 2 mL of ethanol that was then combined with a 2 mL ethanol solution containing 36.9 mg of 4,6-diBr res (2:1 molar ratio). The cap was removed, and the vial was placed on the benchtop to allow slow evaporation. Single crystals suitable for X-ray diffraction were obtained within 2 days. When allowed to evaporate to dryness, a small amount excess SB was observed.

Crystallization of (4,6-diBr res)·2(PAB)

Cocrystals of (4,6-diBr res)·2(PAB) were synthesized by dissolving 50.0 mg of PAB in 2 mL of ethanol that was then combined with a 2 mL ethanol solution containing 37.3 mg of 4,6-diBr res (2:1 molar ratio). The cap was removed, and the vial was placed on the benchtop to allow slow evaporation. Single crystals suitable for X-ray diffraction were obtained within 2 days.

Crystallization of (4,6-diBr res)·(SB)·(PAB)

Lastly, the mixed cocrystal (4,6-diBr res)·(SB)·(PAB) was synthesized by dissolving 25.0 mg of SB and 25.0 mg of PAB both in 2 mL of ethanol then combined with a 2 mL ethanol solution containing 37.1 mg of 4,6-diBr res (1:1:1 molar ratio). The cap was removed, and the vial was placed on the benchtop to allow slow evaporation. As before, single crystals suitable for X-ray diffraction were obtained within 2 days.

Additional mixed cocrystal experiments

In general, mixed cocrystals have been synthesized using unequal ratios of isosteric components. The formation of additional mixed cocrystals at a ratio of 0.75:0.25 and 0.25:0.75 with respect to SB:PAB was also attempted. In particular, the 0.75:0.25 ratio of SB:PAB was attempted by dissolving 37.5 mg of SB, 12.5 mg of PAB, and 37.1 mg of 4,6-diBr res each in 2 mL of ethanol and then the solutions were combined. The 0.25:0.75 ratio of SB:PAB was attempted by dissolving 12.5 mg of SB, 37.5 mg of PAB, and 37.1 mg of 4,6-diBr res each in 2 mL of ethanol and the solutions were combined. The cap was removed, and the vial was placed on the benchtop to allow slow evaporation. In both cases, only binary cocrystals were identified by screening several crystals via single-crystal X-ray diffraction.

2. X-ray Diffraction Information and Data Tables

Data were collected on a Bruker D8 VENTURE DUO diffractometer equipped with a IμS 3.0 microfocus source operated at 75 W (50 kV, 1.5 mA) to generate Mo Kα radiation (λ = 0.71073 Å) and a PHOTON III detector. Crystals were transferred from the vial and placed on a glass slide in type NVH immersion oil by Cargille. A Zeiss Stemi 305 microscope was used to identify a suitable specimen for X-ray diffraction from a representative sample of the material. The selected crystal and a small amount of the oil were collected on a MiTeGen 100-micron MicroLoop and transferred to the instrument where it was placed under a nitrogen stream (Oxford 800 series) at 290 K. The sample was optically centered with the aid of a video camera to ensure that no translations were observed as the crystal was rotated through all positions. A unit cell collection was then carried out. After it was determined that the unit cell was not present in the CCDC database a data collection strategy was calculated by *APEX5*.[4] The crystal was measured for size, morphology, and color. After the initial data collection, subsequent data collections were conducted after the temperature of the cold stream was reduced at a rate of 4 K/minute to the desired temperature. After data collection, the unit cell was re-determined using a subset of the full data collection. Intensity data were corrected for Lorentz, polarization, and background effects using the *APEX5*.[4] A numerical absorption correction was applied based on a Gaussian integration over a multifaceted crystal and followed by a semi-empirical correction for adsorption applied using *SADABS*.[4] The program *SHELXT*[5] was used for the initial structure solution and *SHELXL*[6] was used for refinement of the structure. Both programs were utilized within the OLEX2 software.[7] Hydrogen atoms bound to carbon and oxygen atoms were located in the difference Fourier map and were geometrically constrained using the appropriate AFIX commands.

Special Refinement Details

For crystal structures (4,6-diBr res)·2(SB) and (4,6-diBr res)·(SB)·(PAB) there were disordered atom sites that were treated as split sites. Details are listed below for each structure and occupancies for the disordered sites at each temperature.

Refinement for (4,6-diBr res)·2(SB)

In this structure, one ethylene moiety (C12 and C13) was undergoing pedal motion, and these atoms were modeled as split sites (A and B). To help maintain reasonable bond length and

ADP values for the disordered sites, SIMU, RIGU, and free variable DFIX restraints were applied. The structural model of the 290 K data was then used as a starting point for the data collected at other temperatures. At a temperature of 230 K and below, there was no longer an indication of a disordered ethylene moiety, and it was removed from the model. For this structure, attempts to also include disorder of the phenyl ring (C14 < C19) did not produce stable split sites even with SIMU and RIGU restraints applied.

Temperature (K)	Occupancy of A sites	Occupancy of B sites
290	0.95	0.05
270	0.96	0.04
250	0.98	0.02

Refinement for (4,6-diBr res)·(SB)·(PAB)

In this structure, 4-stilbazole and 4-(phenylethynyl)pyridine molecules occupy the same crystallographic space within the structure. In most cases, it is reasonable to discern the differences in the electron density between the ethylene and acetylene moieties. However, how those bridging moieties affect the location of the phenyl or pyridyl rings is more complicated and nuanced. In this particular case, the hydrogen bonding resorcinol molecule to the pyridyl rings forces a similar configuration regardless of the bridging moiety. For the phenyl rings, however, with the 290 K data, both rings were modeled as split sites with RIGU and SIMU restraints applied. After initial refinements, only the ring containing carbon atoms C14 < C19 maintained reasonable ring configurations and demonstrated reasonable split sites. For the phenyl ring containing carbon atoms C27 < C32, the refined split sites were not able to maintain reasonable split sites and were modeled as single sites. For the partial occupancies and disorder sites, RIGU, SIMU, and free variable DFIX restraints were applied. The structural model of the 290 K data was created first and then used as a starting point for the data collected at other temperatures.

Temperature (K)	Occupancy of acetylene (C12 < C19)	Occupancy of ethylene (C12 < C19)	Occupancy of acetylene (C25 < C26)	Occupancy of ethylene (C25 < C26)
290	0.40	0.60	0.33	0.67
270	0.40	0.60	0.34	0.66
250	0.40	0.60	0.35	0.65
230	0.37	0.63	0.34	0.66
210	0.37	0.63	0.36	0.64
190	0.36	0.64	0.33	0.67

Table S1. X-ray data for (4,6-diBr res)·2(SB) at 290, 270, and 250 K.

compound formula	$C_{32}H_{26}Br_2N_2O_2$	$C_{32}H_{26}Br_2N_2O_2$	$C_{32}H_{26}Br_2N_2O_2$
formula mass	630.37	630.37	630.37
crystal system	Triclinic	Triclinic	Triclinic
space group	$P\bar{1}$	$P\bar{1}$	$P\bar{1}$
a/Å	10.894(6)	10.859(4)	10.828(4)
b/Å	11.122(6)	11.115(4)	11.110(3)
c/Å	11.660(8)	11.650(5)	11.643(4)
α/°	92.486(11)	92.382(9)	92.267(11)
β/°	96.818(14)	96.791(11)	96.759(13)
γ/°	91.889(13)	91.928(12)	91.968(11)
V/Å^3	1400.5(14)	1394.0(9)	1388.8(8)
ρ_{calc}/g cm^{-3}	1.495	1.502	1.507
T/K	290	270	250
Z	2	2	2
radiation type	MoKα (λ = 0.71073)	MoKα (λ = 0.71073)	MoKα (λ = 0.71073)
absorption coefficient, μ/mm^{-1}	2.926	2.940	2.951
crystal size/mm^3	0.196 × 0.175 × 0.163	0.196 × 0.175 × 0.163	0.196 × 0.175 × 0.163
no. of reflections measured	46592	46402	46246
no. of independent reflections	5673	5639	5618
no. of reflection (I > 2σ(I))	4020	4131	4229
R_{int}	0.0929	0.0886	0.0849
R_1 (I > 2σ(I))	0.0368	0.0330	0.0324
$wR(F^2)$ (I > 2σ(I))	0.0695	0.0663	0.0668
R_1 (all data)	0.0655	0.0566	0.0535
$wR(F^2)$ (all data)	0.0795	0.0745	0.0743
Goodness-of-fit	1.011	1.008	1.018
CCDC deposition number	2420438	2420439	2420440

Table S2. X-ray data for (4,6-diBr res)·2(SB) at 230, 210, and 190 K.

compound formula	$C_{32}H_{26}Br_2N_2O_2$	$C_{32}H_{26}Br_2N_2O_2$	$C_{32}H_{26}Br_2N_2O_2$
formula mass	630.37	630.37	630.37
crystal system	Triclinic	Triclinic	Triclinic
space group	$P\bar{1}$	$P\bar{1}$	$P\bar{1}$
a/Å	10.797(5)	10.766(5)	10.741(5)
b/Å	11.105(5)	11.097(5)	11.091(5)
c/Å	11.636(7)	11.629(7)	11.623(6)
α/°	92.156(12)	92.048(11)	91.955(10)
β/°	96.727(11)	96.699(13)	96.665(12)
γ/°	91.992(11)	92.013(11)	92.024(11)
V/Å^3	1383.5(12)	1377.8(12)	1373.4(12)
ρ_{calc}/g cm^{-3}	1.513	1.519	1.524
T/K	230	210	190
Z	2	2	2
radiation type	MoKα (λ = 0.71073)	MoKα (λ = 0.71073)	MoKα (λ = 0.71073)
absorption coefficient, μ/mm^{-1}	2.962	2.974	2.984
crystal size/mm^3	0.196 × 0.175 × 0.163	0.196 × 0.175 × 0.163	0.196 × 0.175 × 0.163
no. of reflections measured	46047	45868	45706
no. of independent reflections	5602	5578	5557
no. of reflection (I > 2σ(I))	4325	4387	4459
R_{int}	0.0833	0.0814	0.0787
R_1 (I > 2σ(I))	0.0317	0.0304	0.0299
$wR(F^2)$ (I > 2σ(I))	0.0651	0.0619	0.0608
R_1 (all data)	0.0499	0.0464	0.0442
$wR(F^2)$ (all data)	0.0714	0.0674	0.0656
Goodness-of-fit	1.021	1.022	1.018
CCDC deposition number	2420441	2420442	2420443

Table S3. X-ray data for (4,6-diBr res)·2(PAB) at 290, 270, and 250 K.

compound formula	$C_{32}H_{22}Br_2N_2O_2$	$C_{32}H_{22}Br_2N_2O_2$	$C_{32}H_{22}Br_2N_2O_2$
formula mass	626.33	626.33	626.33
crystal system	Monoclinic	Monoclinic	Monoclinic
space group	$P2_1/c$	$P2_1/c$	$P2_1/c$
a/Å	13.7221(13)	13.7170(12)	13.7103(12)
b/Å	19.6785(19)	19.6387(18)	19.5964(17)
c/Å	10.7022(9)	10.6868(8)	10.6712(8)
α/°	90	90	90
β/°	102.145(2)	102.276(2)	102.412(2)
γ/°	90	90	90
V/Å^3	2825.2(5)	2813.0(4)	2800.0(4)
ρ_{calc}/g cm^{-3}	1.473	1.479	1.486
T/K	290	270	250
Z	4	4	4
radiation type	MoKα (λ = 0.71073)	MoKα (λ = 0.71073)	MoKα (λ = 0.71073)
absorption coefficient, μ/mm^{-1}	2.900	2.913	2.927
crystal size/mm^3	0.147 × 0.14 × 0.137	0.147 × 0.14 × 0.137	0.147 × 0.14 × 0.137
no. of reflections measured	45582	45254	45009
no. of independent reflections	5357	5338	5311
no. of reflection (I > 2σ(I))	3492	3611	3726
R_{int}	0.0763	0.0769	0.0752
R_1 (I > 2σ(I))	0.0370	0.0357	0.0348
$wR(F^2)$ (I > 2σ(I))	0.0631	0.0622	0.0643
R_1 (all data)	0.0741	0.0687	0.0646
$wR(F^2)$ (all data)	0.0737	0.0717	0.0734
Goodness-of-fit	1.003	0.998	1.011
CCDC deposition number	2420444	2420445	2420446

Table S4. X-ray data for (4,6-diBr res)·2(PAB) at 230, 210, and 190 K.

compound formula	$C_{32}H_{22}Br_2N_2O_2$	$C_{32}H_{22}Br_2N_2O_2$	$C_{32}H_{22}Br_2N_2O_2$
formula mass	626.33	626.33	626.33
crystal system	Monoclinic	Monoclinic	Monoclinic
space group	$P2_1/c$	$P2_1/c$	$P2_1/c$
a/Å	13.7063(11)	13.6982(11)	13.6922(10)
b/Å	19.5596(17)	19.5139(16)	19.4698(15)
c/Å	10.6580(8)	10.6429(7)	10.6293(7)
α/°	90	90	90
β/°	102.548(2)	102.668(2)	102.781(2)
γ/°	90	90	90
V/Å^3	2789.1(4)	2775.7(4)	2763.4(3)
ρ_{calc}/g cm^{-3}	1.492	1.499	1.505
T/K	230	210	190
Z	4	4	4
radiation type	MoKα (λ = 0.71073)	MoKα (λ = 0.71073)	MoKα (λ = 0.71073)
absorption coefficient, μ/mm^{-1}	2.938	2.952	2.965
crystal size/mm^3	0.147 × 0.14 × 0.137	0.147 × 0.14 × 0.137	0.147 × 0.14 × 0.137
no. of reflections measured	44849	44677	44512
no. of independent reflections	5288	5262	5242
no. of reflection (I > 2σ(I))	3829	3937	3982
R_{int}	0.0734	0.0745	0.0732
R_1 (I > 2σ(I))	0.0341	0.0334	0.0321
$wR(F^2)$ (I > 2σ(I))	0.0612	0.0596	0.0575
R_1 (all data)	0.0600	0.0560	0.0533
$wR(F^2)$ (all data)	0.0689	0.0664	0.0639
Goodness-of-fit	1.019	1.036	1.035
CCDC deposition number	2420447	2420448	2420449

Table S5. X-ray data for (4,6-diBr res)·(SB)·(PAB) at 290, 270, and 250 K.

compound formula	$C_{32}H_{24.55}Br_2N_2O_2$	$C_{32}H_{24.52}Br_2N_2O_2$	$C_{32}H_{24.53}Br_2N_2O_2$
formula mass	628.90	628.87	628.88
crystal system	Triclinic	Triclinic	Triclinic
space group	$P\bar{1}$	$P\bar{1}$	$P\bar{1}$
a/Å	10.9453(7)	10.9159(6)	10.8860(6)
b/Å	11.0670(6)	11.0588(6)	11.0501(5)
c/Å	11.7158(7)	11.7098(7)	11.7037(7)
α/°	92.186(2)	92.098(2)	91.998(2)
β/°	97.370(2)	97.391(2)	97.416(2)
γ/°	91.752(2)	91.784(2)	91.813(2)
V/Å^3	1405.50(14)	1399.97(14)	1394.30(13)
ρ_{calc}/g cm^{-3}	1.486	1.492	1.498
T/K	290	270	250
Z	2	2	2
radiation type	MoKα (λ = 0.71073)	MoKα (λ = 0.71073)	MoKα (λ = 0.71073)
absorption coefficient, μ/mm^{-1}	2.915	2.927	2.939
crystal size/mm^3	0.318 × 0.255 × 0.155	0.318 × 0.255 × 0.155	0.318 × 0.255 × 0.155
no. of reflections measured	41640	41458	50027
no. of independent reflections	5250	5222	6848
no. of reflection (I > 2σ(I))	3898	4037	4819
R_{int}	0.0740	0.0698	0.0772
R_1 (I > 2σ(I))	0.0346	0.0341	0.0362
$wR(F^2)$ (I > 2σ(I))	0.0741	0.0721	0.0770
R_1 (all data)	0.0568	0.0519	0.0650
$wR(F^2)$ (all data)	0.0830	0.0794	0.870
Goodness-of-fit	1.010	1.017	1.020
CCDC deposition number	2420450	2420451	2420452

Table S6. X-ray data for (4,6-diBr res)·(SB)·(PAB) at 230, 210, and 190 K.

compound formula	$C_{32}H_{24.57}Br_2N_2O_2$	$C_{32}H_{24.54}Br_2N_2O_2$	$C_{32}H_{24.63}Br_2N_2O_2$
formula mass	628.93	628.89	628.99
crystal system	Triclinic	Triclinic	Triclinic
space group	$P\bar{1}$	$P\bar{1}$	$P\bar{1}$
a/Å	10.8565(6)	10.8319(5)	10.8084(5)
b/Å	11.0401(5)	11.0319(5)	11.0217(4)
c/Å	11.6972(6)	11.6933(6)	11.6874(6)
α/°	91.8880(10)	91.7910(10)	91.6890(10)
β/°	97.441(2)	97.468(2)	97.496(2)
γ/°	91.8380(10)	91.8610(10)	91.8790(10)
V/Å^3	1388.49(12)	1383.84(11)	1378.84(11)
ρ_{calc}/g cm^{-3}	1.504	1.509	1.515
T/K	230	210	190
Z	2	2	2
radiation type	MoKα (λ = 0.71073)	MoKα (λ = 0.71073)	MoKα (λ = 0.71073)
absorption coefficient, μ/mm^{-1}	2.951	2.961	2.972
crystal size/mm^3	0.318 × 0.255 × 0.155	0.318 × 0.255 × 0.155	0.318 × 0.255 × 0.155
no. of reflections measured	43433	43206	45409
no. of independent reflections	5576	5548	5965
no. of reflection ($I > 2\sigma(I)$)	4416	4532	4885
R_{int}	0.0666	0.0640	0.0640
R_1 ($I > 2\sigma(I)$)	0.0308	0.0298	0.0298
$wR(F^2)$ ($I > 2\sigma(I)$)	0.0680	0.0664	0.0644
R_1 (all data)	0.0463	0.0426	0.0426
$wR(F^2)$ (all data)	0.0740	0.0715	0.0694
Goodness-of-fit	1.024	1.021	1.027
CCDC deposition number	2420453	2420454	2420455

3. Powder X-ray Diffraction Data

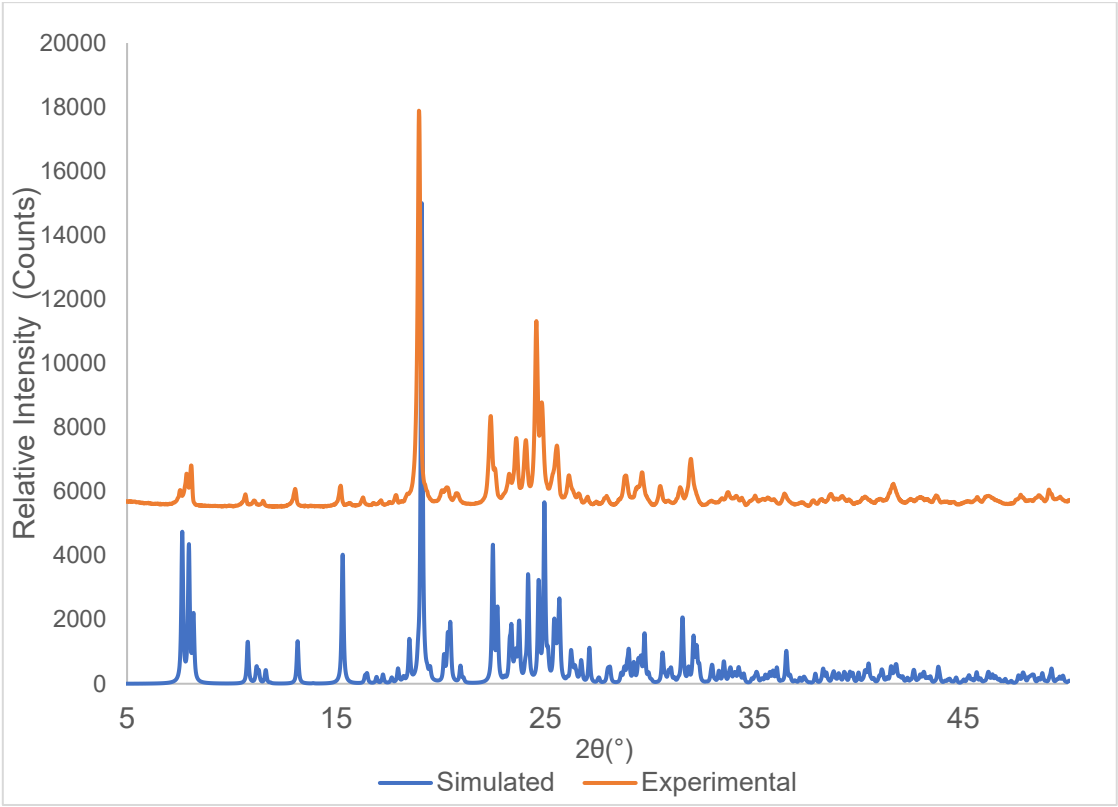

Figure S1. PXRD patterns of (4,6-diBr res)·2(SB) with simulated pattern from single-crystal X-ray data at 290 K and experimental pattern from bulk crystals grown by slow evaporation.

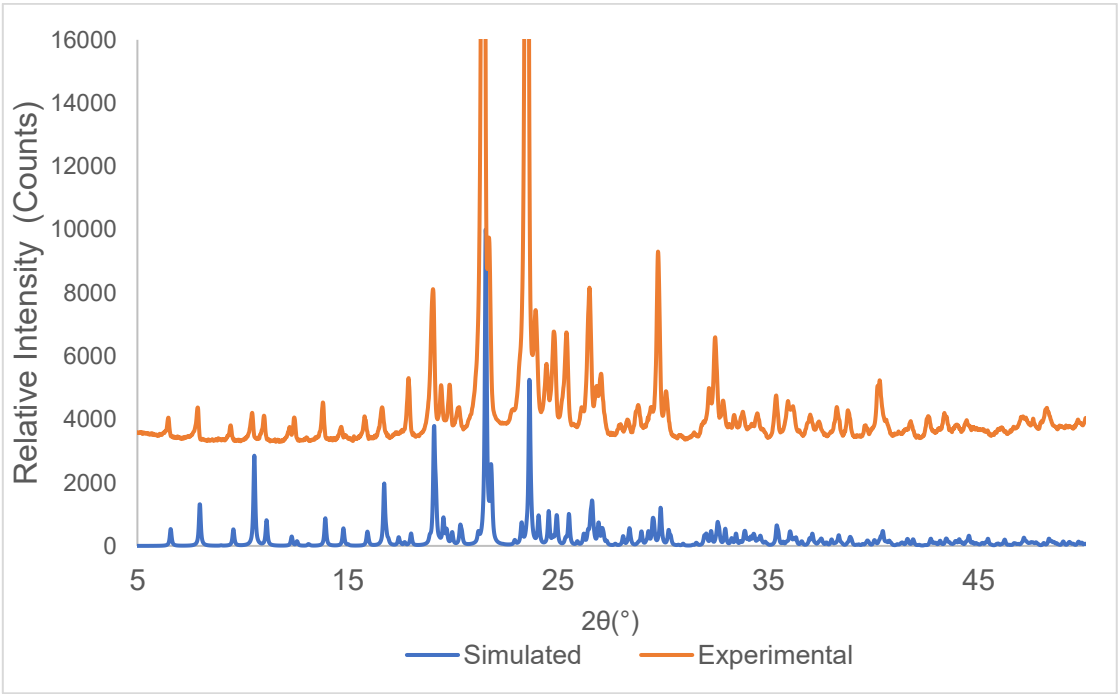

Figure S2. PXRD patterns of (4,6-diBr res)·2(PAB) with simulated pattern from single-crystal X-ray data at 290 K and experimental pattern from bulk crystals grown by slow evaporation.

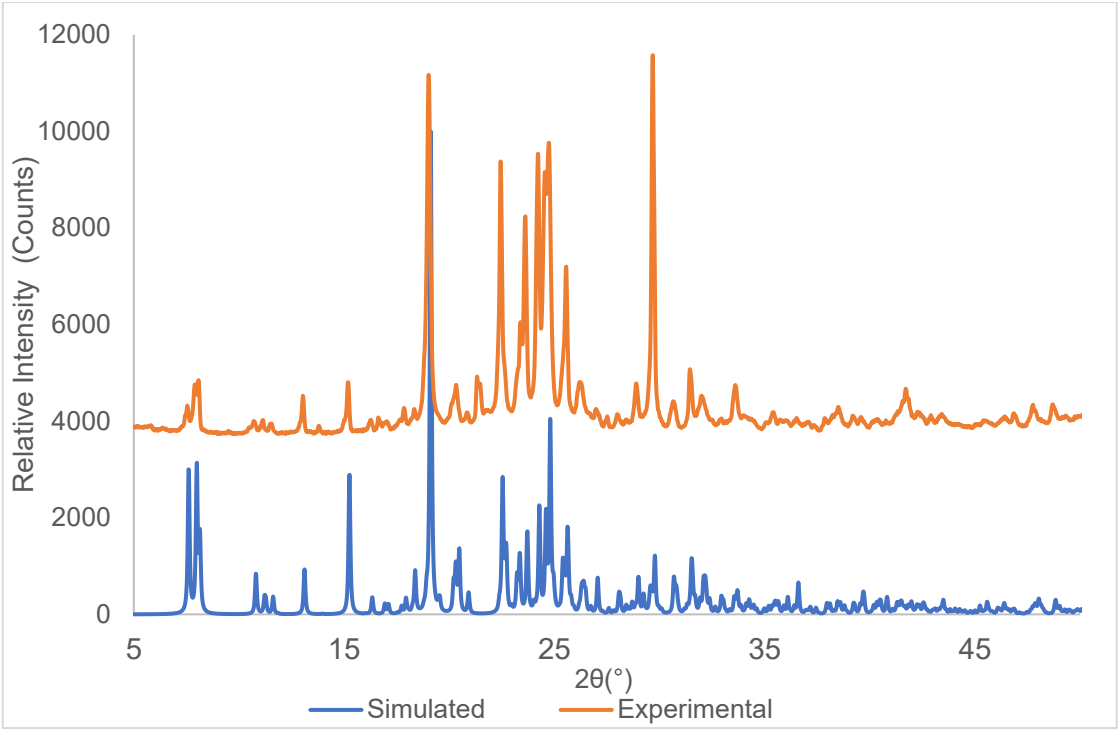

Figure S3. PXRD patterns of (4,6-diBr res)·(SB)·(PAB) with simulated pattern from single-crystal X-ray data at 290 K and experimental pattern from bulk crystals grown by slow evaporation.

4. NMR Spectra

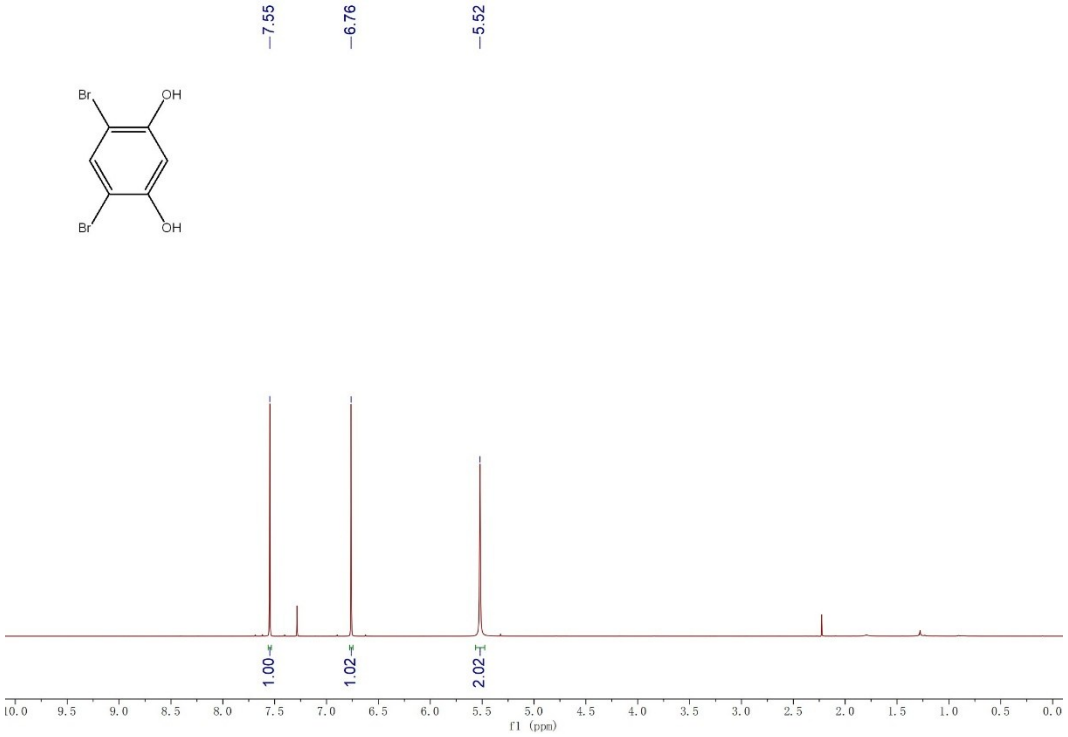

Figure S4. ^{1}H NMR spectrum of 4,6-diBr res.

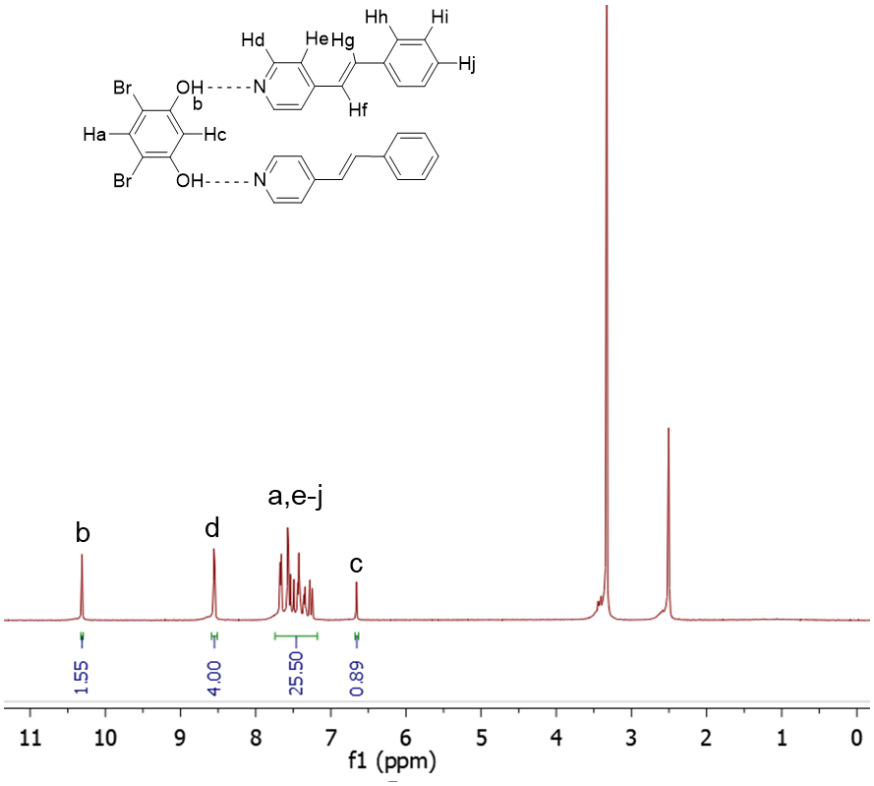

Figure S5. ^{1}H NMR spectrum of (4,6-diBr res)·2(SB).

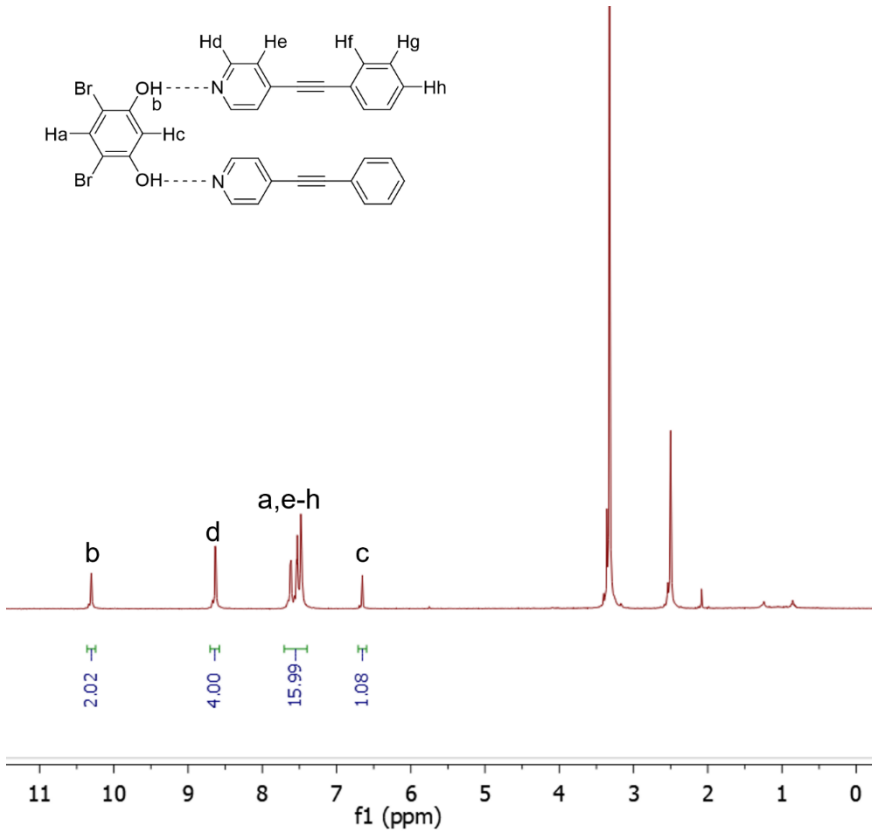

Figure S6. ^{1}H NMR spectrum of (4,6-diBr res)·2(PAB).

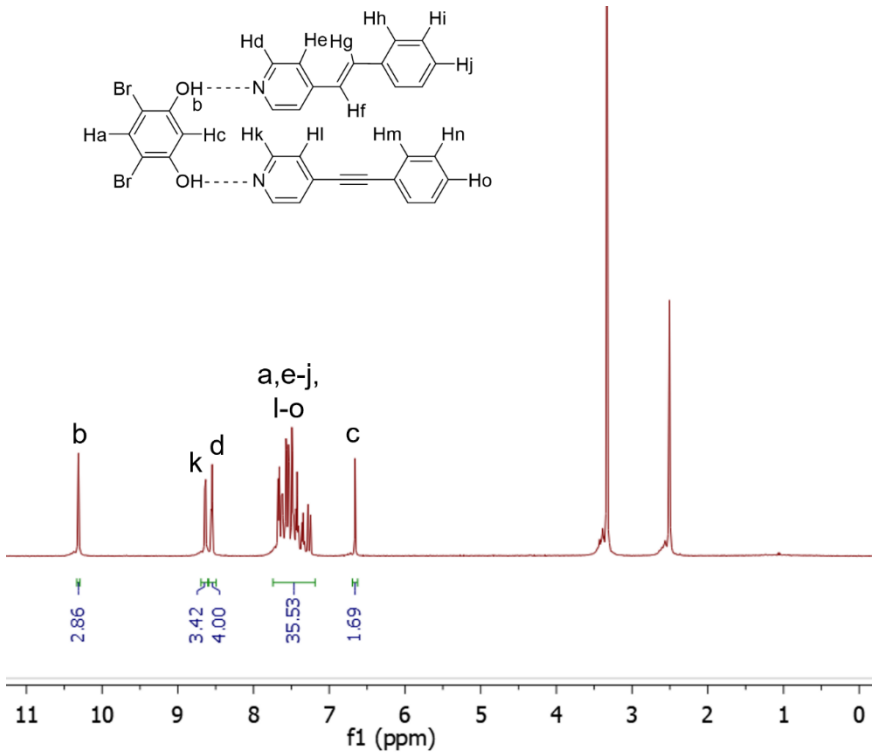

Figure S7. ^{1}H NMR spectrum of (4,6-diBr res)·(SB)·(PAB).

5. Thermal Data (TGA and DSC)

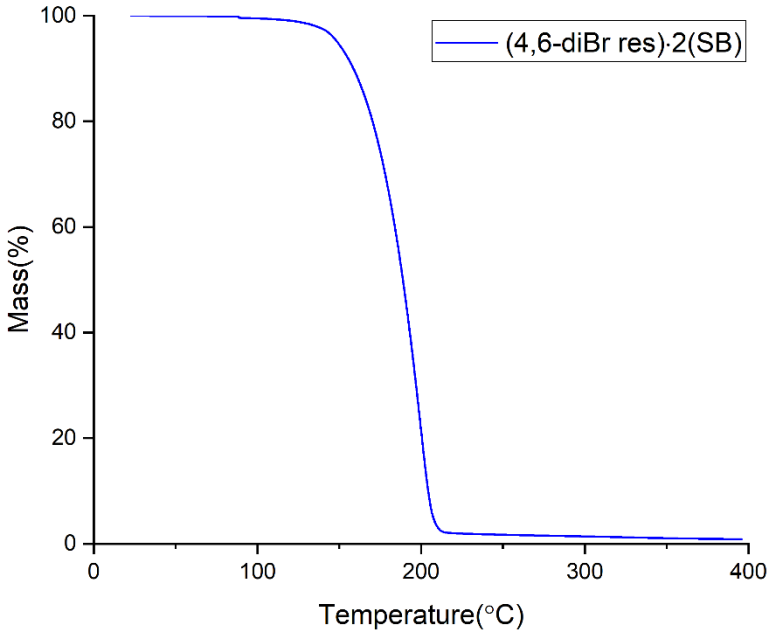

Figure S8. TGA curve of (4,6-diBr res)·2(SB). Decomposition began at ca. 174 °C.

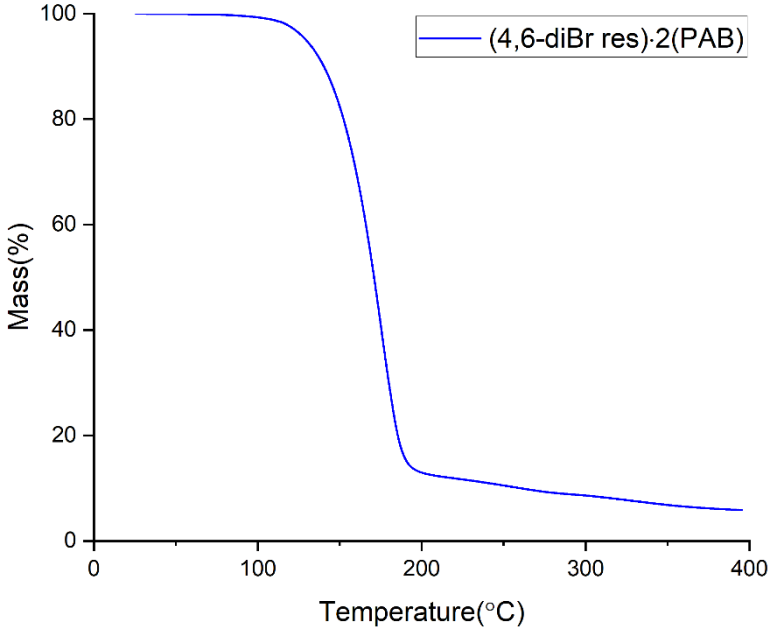

Figure S9. TGA curve of (4,6-diBr res)·2(PAB). Decomposition began at ca. 152 °C.

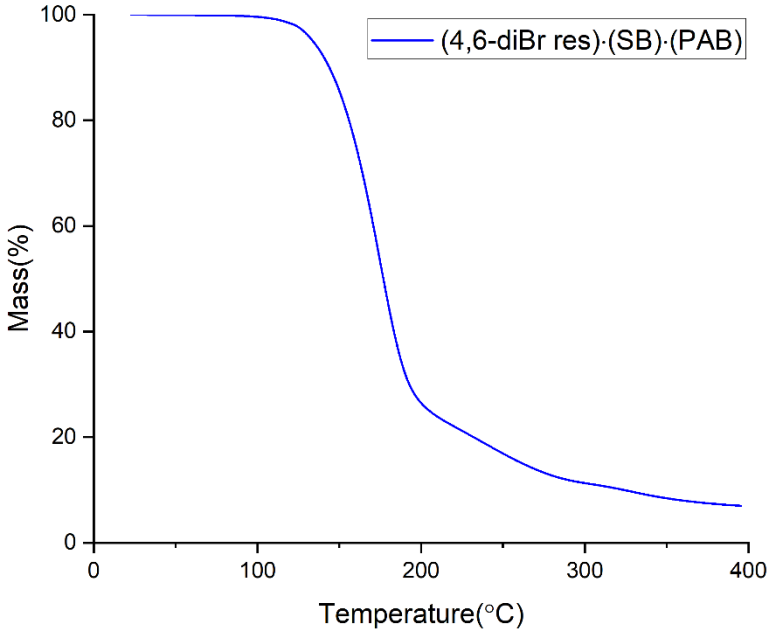

Figure S10. TGA curve of (4,6-diBr res)·(SB)·(PAB). Decomposition began at ca. 150 °C.

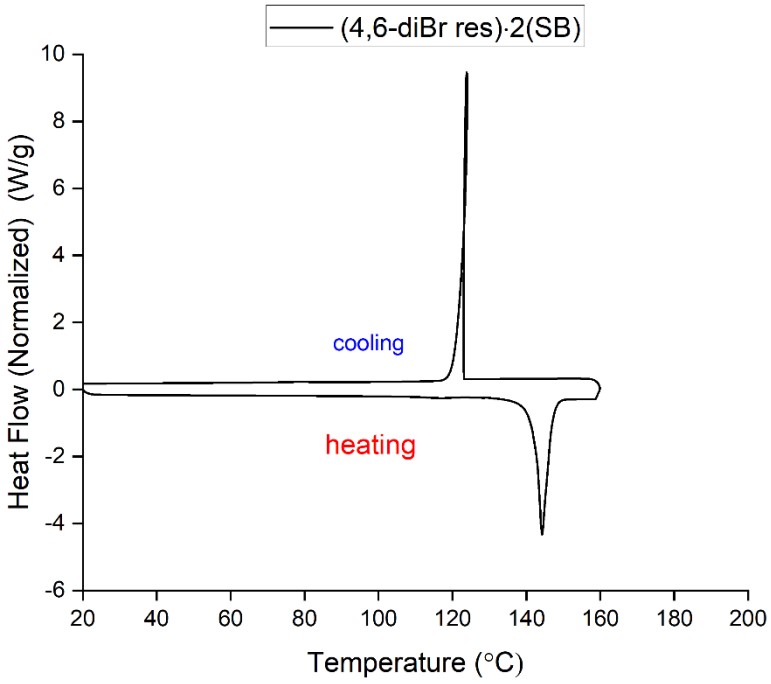

Figure S11. DSC thermogram of (4,6-diBr res)·2(SB) (onset: 142 °C, heating peak: 144 °C, cooling peak: 124 °C).

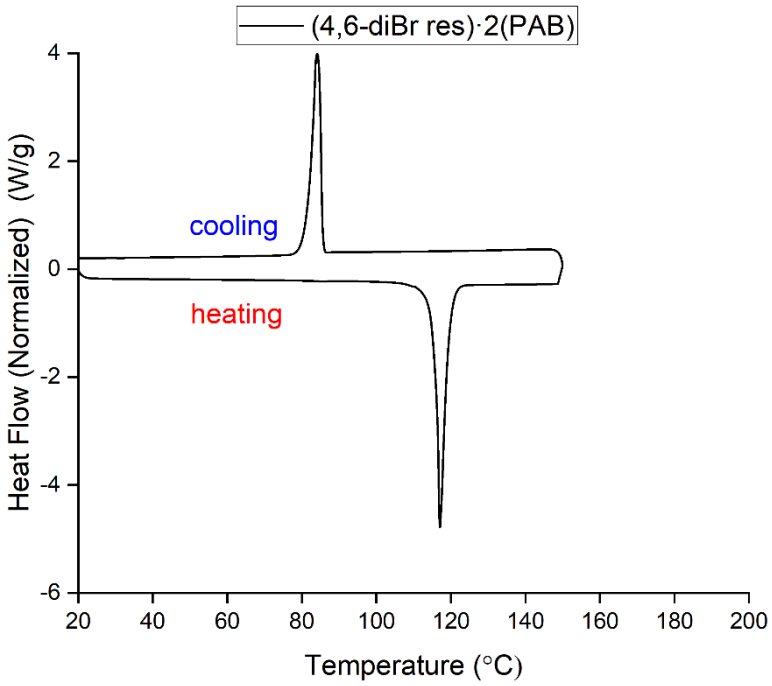

Figure S12. DSC thermogram of (4,6-diBr res)·2(PAB) (onset: 116 °C, heating peak: 117 °C, cooling peak: 84 °C).

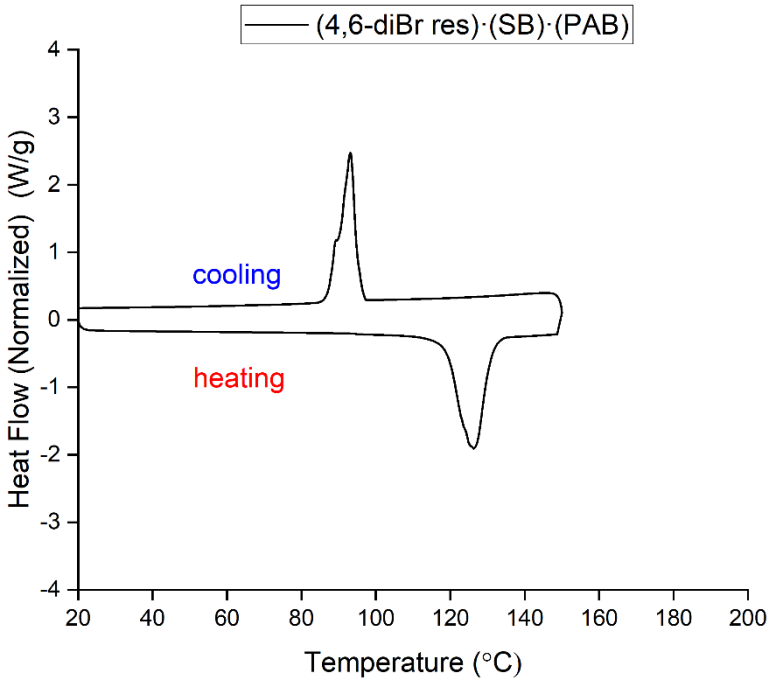

Figure S13. DSC thermogram of (4,6-diBr res)·(SB)·(PAB) (onset: 119 °C, heating peak: 126 °C, cooling peak: 93 °C).

Table S7. Melting point ranges of the solids determined by DSC.

Cocrystal	Melting point (°C)
(4,6-diBr res)·(2SB)	142-144
(4,6-diBr res)·(2PAB)	116-117
(4,6-diBr res)·(SB)·(PAB)	119-126

6. Optical Images of the Cocrystals

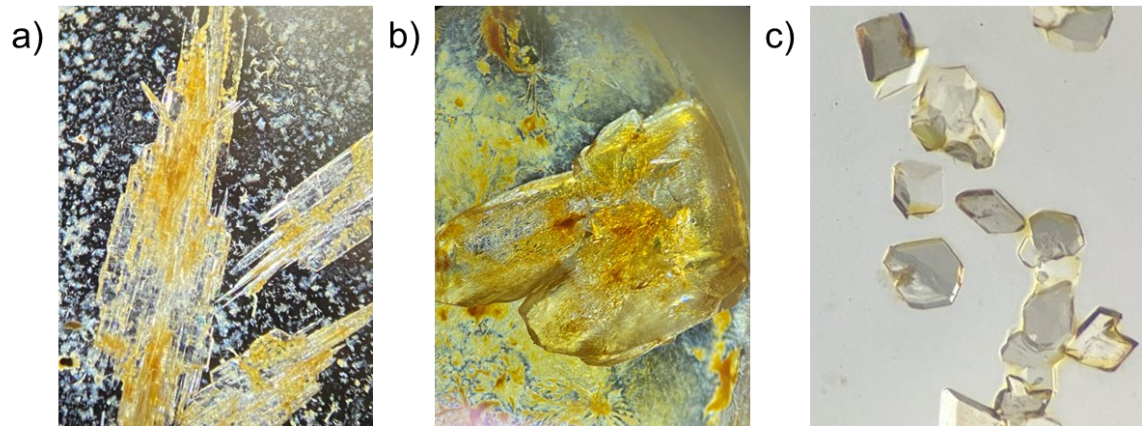

Figure S14. Optical images of crystals viewed under a stereoscope: a) (4,6-diBr res)·2(SB), b) (4,6-diBr res)·2(PAB), and c) (4,6-diBr res)·(SB)·(PAB).

7. Electrostatic Potential Energy Calculations

The Spartan´20 molecular modeling program with density functional theory at the B3LYP/6-311++G** level[8] was used for the calculations. Each molecule was drawn and then locked in the conformation seen in the crystal structures before performing the structural optimization. The electrostatic potential energy surface was calculated for each molecule.

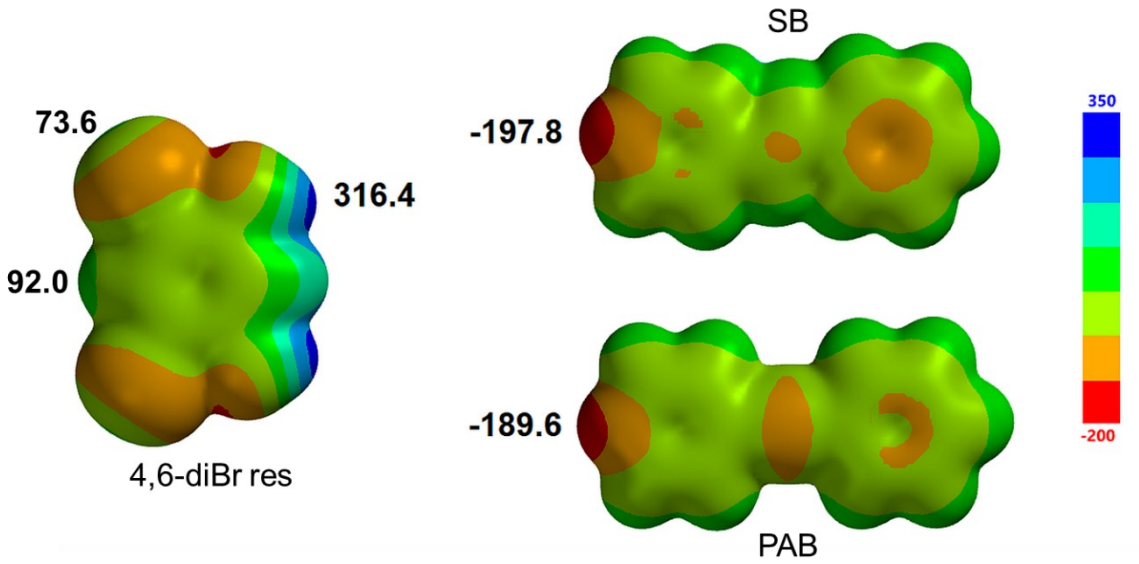

Figure S15. Molecular electrostatic potential energy surface for 4,6-diBr res, SB, and PAB. The unit for the scale is in kJ/mol.

8. Thermal Expansion Data and Intermolecular Interaction Distances

The TE coefficients were calculated using PASCal.[9] The unit cell parameters from the crystallographic data sets collected from 290-190 K were used for the TE calculations (Table S1-S6).

Table S8. TE coefficients for the cocrystals. Errors are denoted in parentheses and approximate crystallographic axes are denoted in brackets.

Cocrystal	α_{X_1} (MK^{-1}) [axis]	α_{X_2} (MK^{-1}) [axis]	α_{X_3}(MK^{-1}) [axis]	α_V(MK^{-1})
(4,6-diBr res)·2(SB)	-20 (1) [0 1 1]	70 (1) [-1 3 -3]	145 (3) [1 0 0]	196 (5)
(4,6-diBr res)·2(PAB)	-4 (1) [4 0 -3]	106 (1) [0 1 0]	120 (1) [1 0 2]	223 (1)
(4,6-diBr res) ·(SB)·(PAB)	-14 (1) [0 1 1]	76 (1) [0 4 -3]	130 (3) [7 0 1]	194 (3)

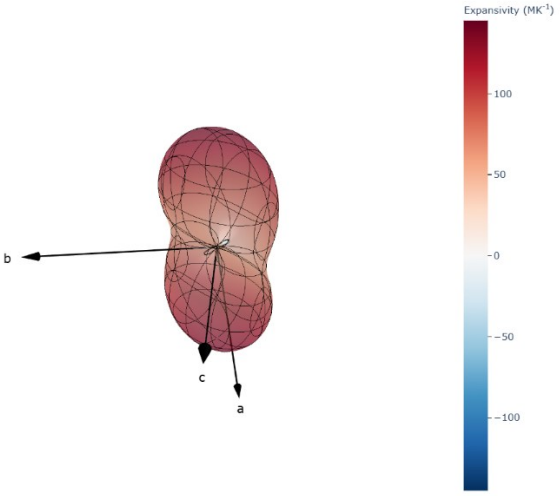

Figure S16. Thermal expansivity indicatrix for (4,6-diBr res)·2(SB).

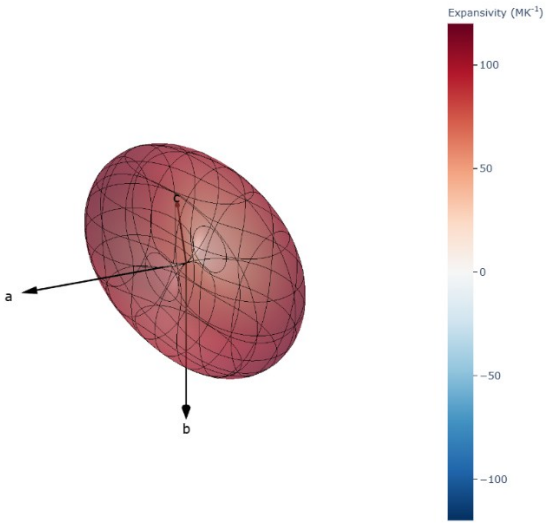

Figure S17. Thermal expansivity indicatrix for (4,6-diBr res)·2(PAB).

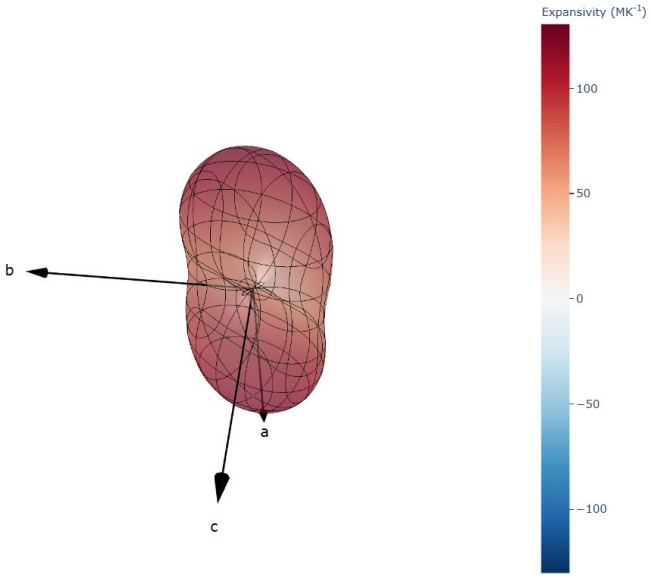

Figure S18. Thermal expansivity indicatrix for (4,6-diBr res)·(SB)·(PAB).

Table S9. Intermolecular interaction distances that contribute to the TE in the complexes.

X_1:

Cocrystal	O-H···N (Å) 290 K	O-H···N (Å) 190 K	Δ (Å)
(4,6-diBr res)·2(SB)	2.690 2.689	2.687 2.688	0.003 0.001
(4,6-diBr res)·2(PAB)	2.749 2.729	2.750 2.724	-0.001 0.005
(4,6-diBr res)·(SB)·(PAB)	2.697 2.699	2.684 2.691	0.013 0.008

Cocrystal	∠O-H···N (˚) 290 K	∠O-H···N (˚) 190 K	Δ (˚)
(4,6-diBr res)·2(SB)	172.69 176.29	172.96 177.59	-0.27 -1.30
(4,6-diBr res)·2(PAB)	170.45 170.98	170.55 170.99	-0.10 -0.01
(4,6-diBr res)·(SB)·(PAB)	172.88 173.10	172.88 177.57	0.00 -4.47

X_2:

Cocrystal	C-H···Br (Å) 290 K	C-H···Br (Å) 190 K	Δ (Å)
(4,6-diBr res)·2(SB)	3.946 3.701 3.823	3.911 3.650 3.798	0.035 0.051 0.025 Avg: 0.037
(4,6-diBr res)·2(PAB)	3.949 3.838 4.200 3.872	3.928 3.787 4.161 3.827	0.021 0.051 0.039 0.045 Avg: 0.039
(4,6-diBr res)·(SB)·(PAB)	3.813 3.744 3.706	3.782 3.713 3.654	0.031 0.031 0.052 Avg: 0.038

Cocrystal	C-H···O (Å) 290 K	C-H···O (Å) 190 K	Δ (Å)
(4,6-diBr res)·2(SB)	3.752	3.740	0.012
(4,6-diBr res)·2(PAB)	3.489	3.442	0.047
(4,6-diBr res)·(SB)·(PAB)	3.694	3.669	0.025

Cocrystal	C-H···π (Å) 290 K	C-H···π (Å) 190 K	Δ (Å)
(4,6-diBr res)·2(SB)	3.683	3.636	0.047
(4,6-diBr res)·2(PAB)	-	-	-
(4,6-diBr res)·(SB)·(PAB)	3.654 3.681	3.614 3.638	0.040 0.043

Cocrystal	C-H···π/C contacts (Å) 290 K	C-H···π/C contacts (Å) 190 K	Δ (Å)
(4,6-diBr res)·2(SB)	-	-	-
(4,6-diBr res)·2(PAB)	3.513 3.426 3.545 4.142	3.452 3.374 3.510 4.103	0.061 0.052 0.035 0.039 Avg: 0.047
(4,6-diBr res)·(SB)·(PAB)	-	-	-

X3:

Cocrystal	π···π (Å) 290 K	π···π (Å) 190 K	Δ (Å)
(4,6-diBr res)·2(SB)	3.875 4.285 4.244	3.841 4.243 4.190	0.034 0.042 0.054
(4,6-diBr res)·2(PAB)	-	-	-
(4,6-diBr res)·(SB)·(PAB)	3.868 4.312 4.215	3.828 4.282 4.165	0.040 0.030 0.050

Cocrystal	C-H···O (Å) 290 K	C-H···O (Å) 190 K	Δ (Å)
(4,6-diBr res)·2(SB)	3.312	3.252	0.060
(4,6-diBr res)·2(PAB)	3.361	3.304	0.057
(4,6-diBr res)·(SB)·(PAB)	3.306	3.226	0.080

Cocrystal	Br···π (Å) 290 K	Br···π (Å) 190 K	Δ (Å)
(4,6-diBr res)·2(SB)	3.474 3.573	3.416 3.497	0.058 0.076
(4,6-diBr res)·2(PAB)	-	-	-
(4,6-diBr res)·(SB)·(PAB)	3.511 3.595	3.434 3.522	0.077 0.073

(4,6-diBr res)·2(PAB)	290 K	190 K	Δ (Å)
Br···Br (Å)	3.838	3.807	0.031
Stacking centroid-centroid (Å)	5.631 4.612 6.257	5.589 4.664 6.256	0.042 -0.052 0.001
C-H···π (Å)	3.838 3.882	3.807 3.838	0.031 0.044

Table S10. Major and minor site occupancies of SB at each temperature for both (4,6-diBr res)·2(SB) and (4,6-diBr res)·(SB)·(PAB).

Temperature	(4,6-diBr res)·2(SB)	(4,6-diBr res)·(SB)·(PAB)
290 K	0.95/0.05	0.60/0.40 0.67/0.33
270 K	0.96/0.04	0.60/0.40 0.66/0.34
250 K	0.98/0.02	0.60/0.40 0.65/0.35
230 K	-	0.63/0.37 0.66/0.34
210 K	-	0.63/0.37 0.64/0.36
190 K	-	0.64/0.36 0.67/0.33

9. Additional Crystal Structure Images

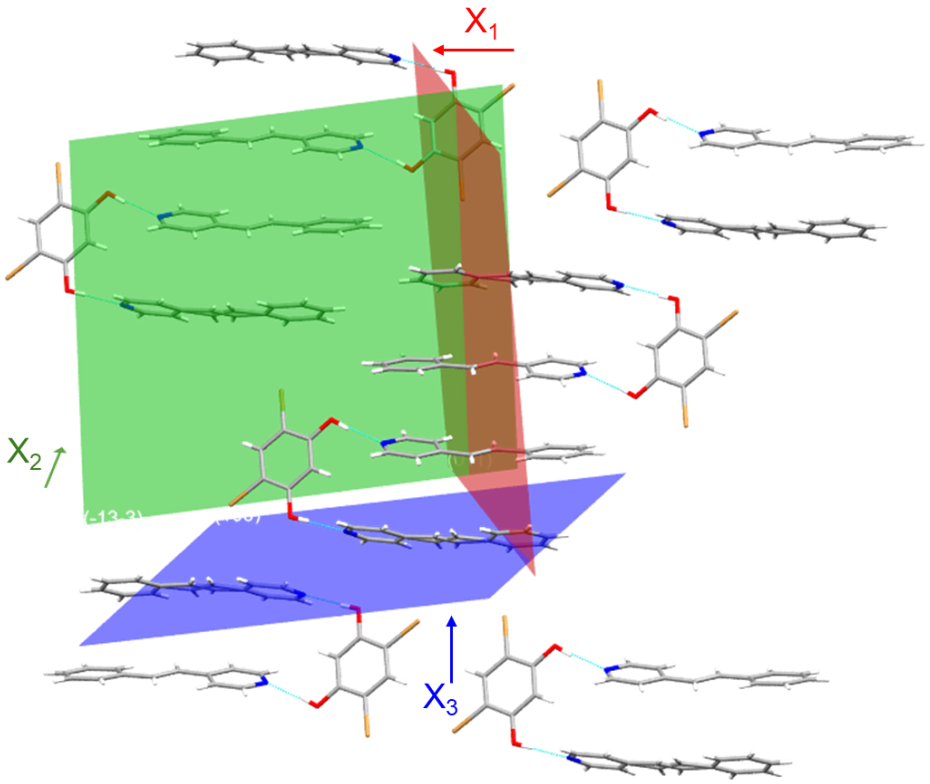

Figure S19. Principal axes of TE for (4,6-diBr res)·2(SB).

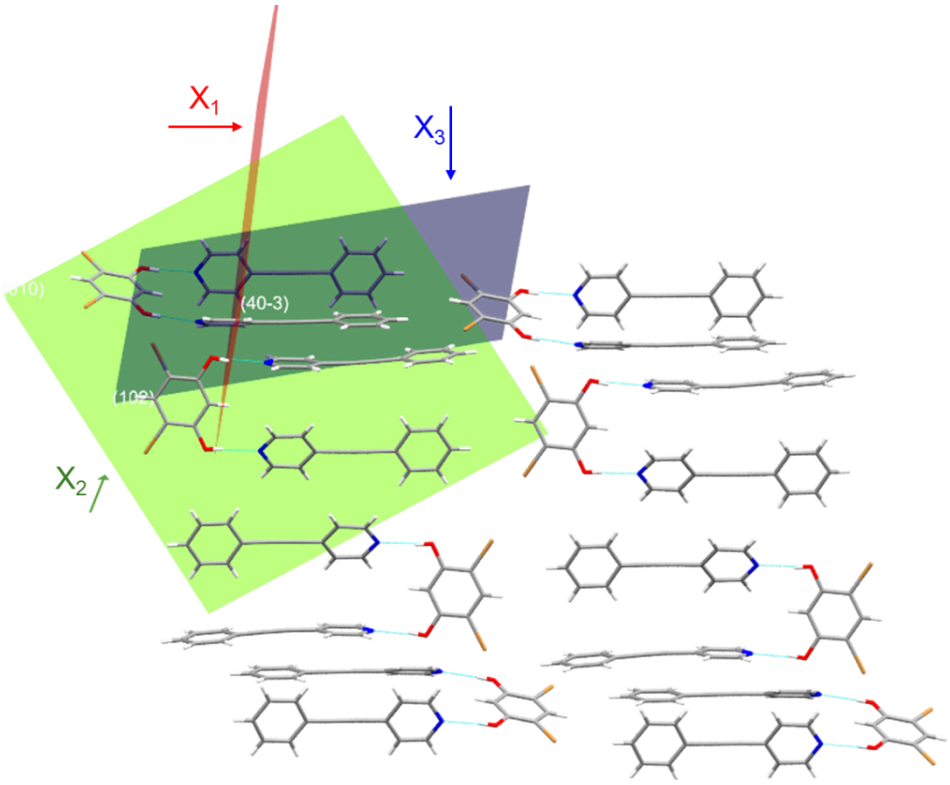

Figure S20. Principal axes of TE for (4,6-diBr res)·2(PAB).

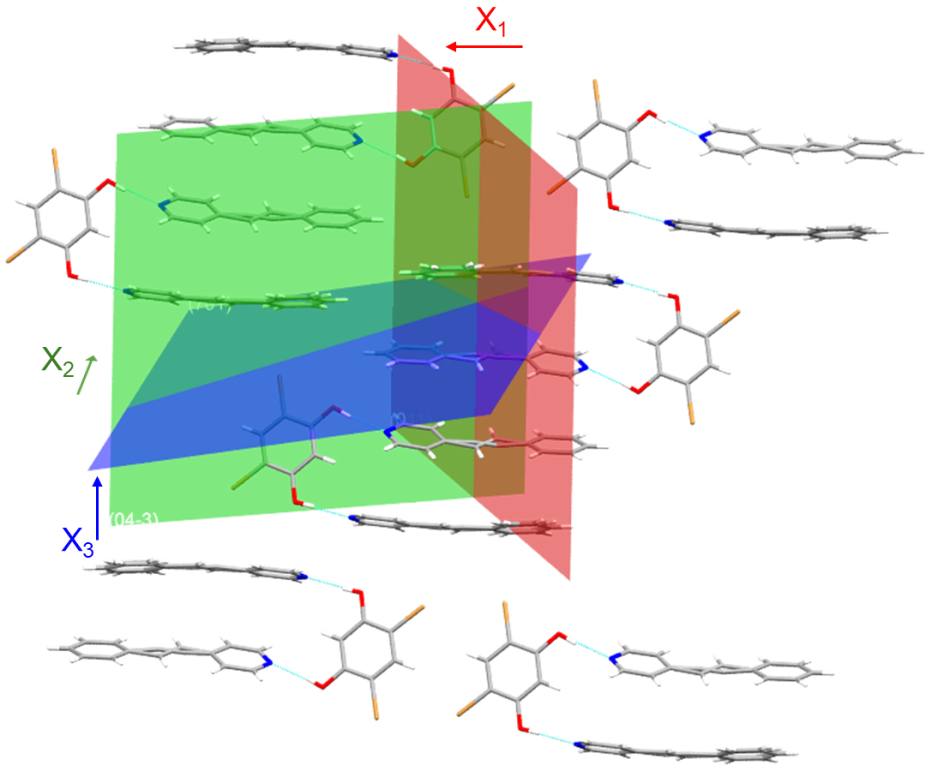

Figure S21. Principal axes of TE for (4,6-diBr res)·(SB)·(PAB).

10. Variation of the Unit Cell Parameters with Temperature

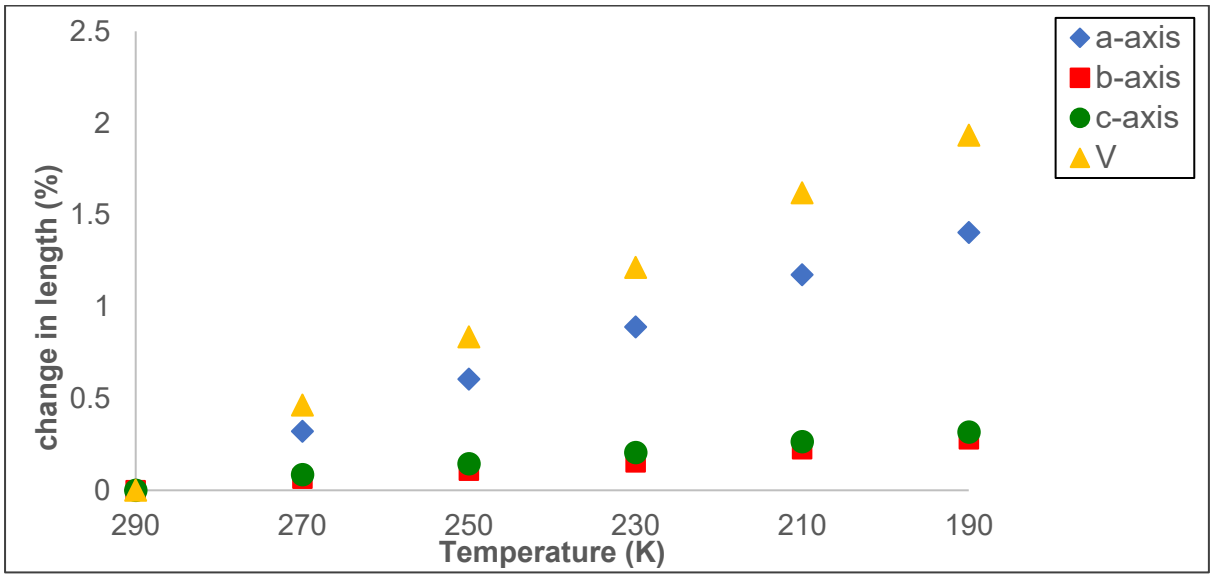

Figure S22. Percent change in length as a function of temperature for (4,6-diBr res)·2(SB).

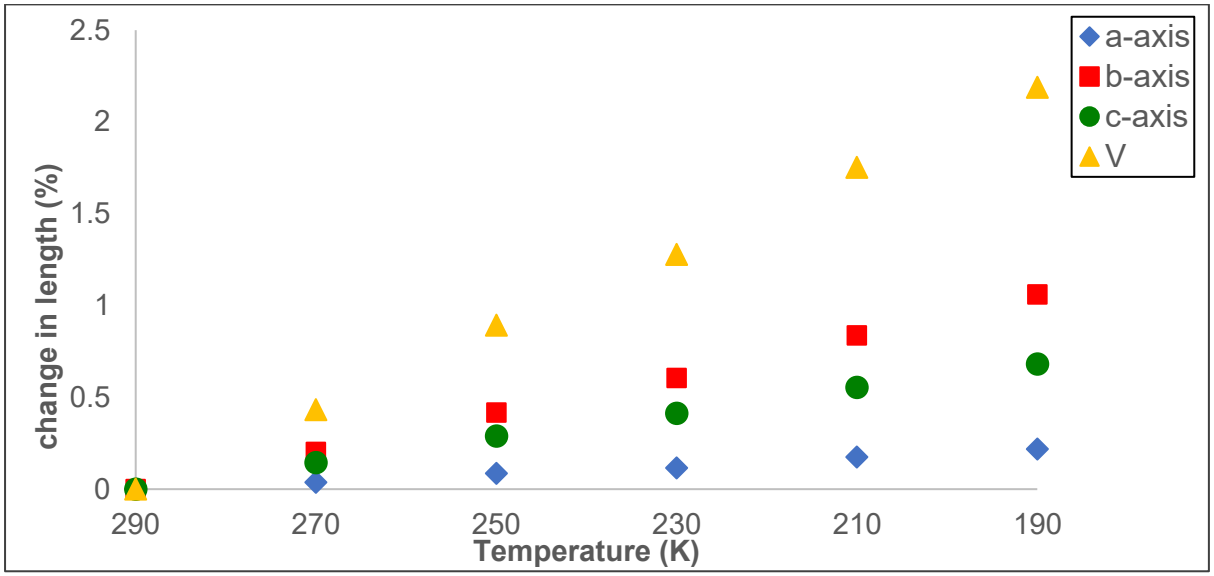

Figure S23. Percent change in length as a function of temperature for (4,6-diBr res)·2(PAB).

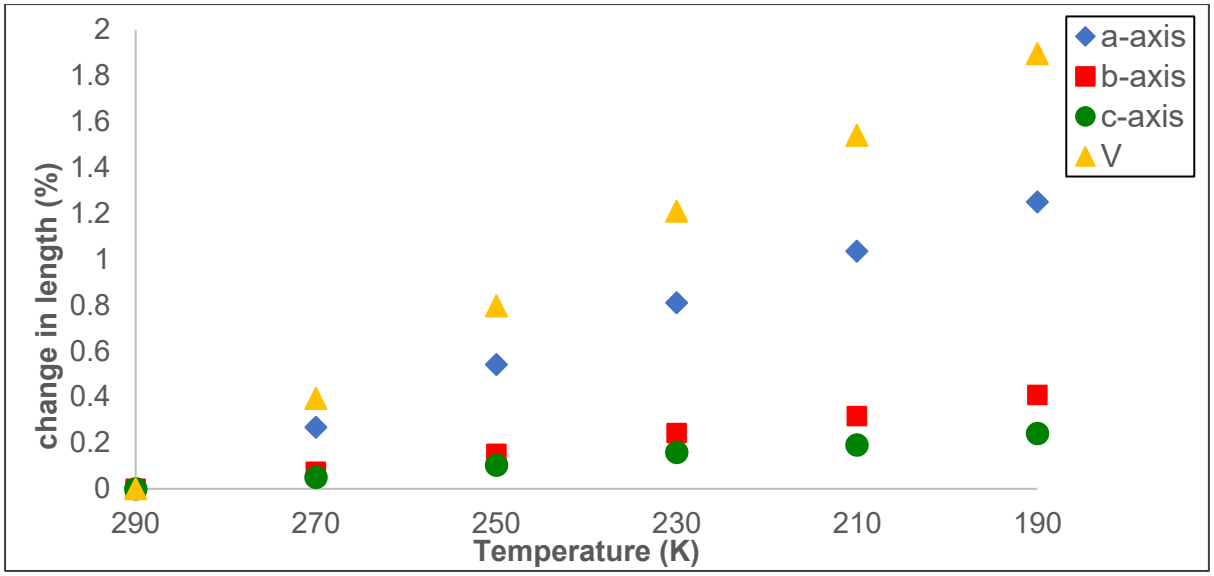

Figure S24. Percent change in length as a function of temperature for (4,6-diBr res)·(SB)·(PAB).

11. References

1. Jin, K.; Yue, B.; Yan, L.; Qiao, R.; Zhao, H.; Zhang, J. Synthesis and Characterization of Poly (5'-hexyloxy-1',4-biphenyl)-b-poly (2',4'-bispropoxysulfonate-1', 4-biphenyl) with High Ion Exchange Capacity for Proton Exchange Membrane Fuel Cell Applications. *Chem. Asian J.* **2022**, *17*, e202200109.

2. George III, G. C.; Unruh, D. K.; Groeneman, R. H.; Hutchins, K. M. Molecular Motion and Ligand Stacking Influence Thermal Expansion Behavior and Argentophilic Forces in Silver Coordination Complexes. *Cryst. Growth Des.* **2022**, *22*, 4538-4545.

3. Hutchins, K. M.; Rupasinghe, T. P.; Ditzler, L. R.; Swenson, D. C.; Sander, J. R.; Baltrusaitis, J.; Tivanski, A. V.; MacGillivray, L. R. Nanocrystals of a metal–organic complex exhibit remarkably high conductivity that increases in a single-crystal-to-single-crystal transformation. *J. Am. Chem. Soc.* **2014**, *136*, 6778-6781.

4. Bruker. APEX5, SAINT and SADABS. 2021 Bruker AXS Inc., Madison, Wisconsin, USA.

5. Sheldrick, G. M. SHELXT - Integrated space-group and crystal-structure determination. *Acta Crystallogr., Sect. A: Found. Adv.* **2015**, *A71*, 3-8.

6. Sheldrick, G. M. Crystal structure refinement with SHELXL. *Acta Crystallogr., Sect. C: Struct. Chem.* **2015**, *C71*, 3-8.

7. Dolomanov, O. V.; Bourhis, L. J.; Gildea, R. J.; Howard, J. A. K.; Puschmann. H. OLEX2: a complete structure solution, refinement and analysis program. *J. Appl. Cryst.* **2009**, *42*, 339-341.

8. *Spartan'20, Version 1.0.1*; Wavefunction, Inc.: Irvine, CA, USA, 2020.

9. Cliffe, M. J.; Goodwin, A. L. PASCal: a principal axis strain calculator for thermal expansion and compressibility determination. *J. Appl. Cryst.* **2012**, *45*, 1321-1329.